Oxo-Centered Mixed-Ligand Triruthenium Complexes Having Redox-Active *N*-Methyl-4,4′-bipyridinium Ions ($mbpy^+$). Reversible Multistep Electrochemical Properties of $[Ru^{III}_2Ru^{II}(\mu_3\text{-}O)(\mu\text{-}CH_3CO_2)_6(mbpy^+)_2(CO)]^{2+}$ and $[Ru^{III}_3(\mu_3\text{-}O)(\mu\text{-}CH_3CO_2)_6(mbpy^+)_2(L)]^{3+}$ (L = H_2O and *N*-Heterocyclic Ligands)

Masaaki Abe,*,†,⊥ Yoichi Sasaki,*,‡ Yasuko Yamada,§ Keiichi Tsukahara,§ Shigenobu Yano,*,§ Tadashi Yamaguchi,† Masato Tominaga,|| Isao Taniguchi,|| and Tasuku Ito*,†

Department of Chemistry, Graduate School of Science, Tohoku University, Aoba-ku, Aramaki, Sendai 980-77, Japan, Division of Chemistry, Graduate School of Science, Hokkaido University, Kita-ku, Sapporo 060, Japan, Department of Chemistry, Faculty of Science, Nara Women's University, Nara 630, Japan, and Department of Applied Chemistry, Faculty of Engineering, Kumamoto University, Kurokami, Kumamoto 860, Japan

Received April 19, 1996[⊗]

A new series of oxo-centered acetate-bridged triruthenium comlexes having two redox-active *N*-methyl-4,4′-bipyridinium ions ($mbpy^+$) have been prepared, and their reversible multistep and multielectron electrochemical properties are reported: $[Ru^{III}_2Ru^{II}(\mu_3\text{-}O)(\mu\text{-}CH_3CO_2)_6(mbpy^+)_2(CO)]^{2+}$ and $[Ru^{III}_3(\mu_3\text{-}O)(\mu\text{-}CH_3CO_2)_6(mbpy^+)_2(L)]^{3+}$ (L = H_2O, pyrazine (pz), pyridine (py), imidazole (Him), and 4-(dimethylamino)pyridine (dmap)). Among these series, the CO complex, $[Ru^{III}_2Ru^{II}(\mu_3\text{-}O)(\mu\text{-}CH_3CO_2)_6(mbpy^+)_2(CO)](ClO_4)_2\cdot 2DMF$ (**1b**·2DMF) was structurally characterized by X-ray crystallography. **1b**·2DMF crystallizes in the monoclinic space group $P2_1/m$ (No. 11) with $a = 8.740(6)$ Å, $b = 32.269(6)$ Å, $c = 10.276(4)$ Å, $\beta = 103.37(5)°$, $V = 2820(2)$ Å^3, $Z = 2$, $d_{calcd} = 1.636$ g cm^{-3}, and $R = 0.071$ ($R_w = 0.074$) for 5277 independent reflections ($|F_o| > 3\sigma(|F_o|)$). The (CO)-Ru···Ru distance (3.410(2) Å) is appreciably longer than the other Ru···Ru distance (3.276(2) Å), indicating that the trinuclear core is in the valence-trapped $Ru^{III}_2Ru^{II}$(CO) oxidation state. The cyclic voltammogram of $[Ru^{III}_2Ru^{II}(\mu_3\text{-}O)(\mu\text{-}CH_3CO_2)_6(mbpy^+)_2(CO)](PF_6)_2$ (**1a**) shows a total of seven reversible one-electron redox steps at $E_{1/2} = +0.90$, $+0.26$, -1.07, -1.17, -1.56, -1.97, and -2.32 V and one irreversible step at $E_{pc} = -2.99$ V *vs* Fc/Fc^+ in a 0.1 M $[(n\text{-}C_4H_9)_4N]PF_6-CH_3CN$ solution (M = mol dm^{-3}). All of the waves are clearly assignable to the triruthenium "$Ru_3(\mu_3\text{-}O)$" core-based or $mbpy^+$ ligand-based processes. The splitting of each ligand-based redox processes ($mbpy^+/mbpy^•$ and $mbpy^•/mbpy^-$) into two one-electron steps indicates that electronic interactions between two terminal ligands occur through the triruthenium cluster core. Other mixed-ligand Ru^{III}_3 analogs also show multistep redox behavior involving a total of eight or nine electrons. While the extent of interactions between ligands is much smaller than that found in the CO complex, it is systematically changed by the nature of L; with more basic L, interactions between two $mbpy^+$ ligands become larger.

Introduction

Oxo-centered triruthenium basic carboxylates of the general formula $[Ru_3(\mu_3\text{-}O)(\mu\text{-}RCO_2)_6L_3]^{n+}$ (RCO_2^- = a carboxylate anion, L = a neutral monodentate ligand such as H_2O and pyridine, $n = 0$, 1)[1−3] serve as a remarkable class of metal clusters due to their reversible multistep and multielectron redox chemistry.[4−15] It has been well established that replacement of one Ru, three terminal ligands (L), and six carboxylate bridges (RCO_2^-) results in a systematic tuning upon redox potentials as well as electronic, magnetic, and ligand-substitution properties.[16−19] Thus, the triruthenium complexes are thought to be a desirable unit for constructing multielectron redox systems that are inherently of interest in designing tunable

† Tohoku University.
‡ Hokkaido University.
§ Nara Women's University.
|| Kumamoto University.
⊥ Present address: Hokkaido University.

⊗ Abstract published in *Advance ACS Abstracts,* October 15, 1996.

(1) Cannon, R. D.; White, R. P. *Prog. Inorg. Chem.* **1988**, *36*, 195−298.
(2) Spencer, A.; Wilkinson, G. *J. Chem. Soc., Dalton Trans.* **1972**, 1570−1577.
(3) Spencer, A.; Wilkinson, G. *J. Chem. Soc., Dalton Trans.* **1974**, 786−792.
(4) Baumann, J. A.; Salmon, D. J.; Wilson, S. T.; Meyer, T. J.; Hatfield, W. E. *Inorg. Chem.* **1978**, *17*, 3342−3350.
(5) Walsh, J. L.; Baumann, J. A.; Meyer, T. J. *Inorg. Chem.* **1980**, *19*, 2145−2151.
(6) Toma, H. E.; Cunha, C. J.; Cipriano, C. *Inorg. Chim. Acta* **1988**, *154*, 63−66.
(7) Toma, H. E.; Cunha, C. J. *Can. J. Chem.* **1989**, *67*, 1632−1635.
(8) Toma, H. E.; Alexiou, D. P. *Electrochim. Acta* **1993**, *38*, 975−980.
(9) Kobayashi, H.; Uryû, N.; Tokiwa, A.; Yamaguchi, T.; Sasaki, Y.; Ito, T. *Bull. Chem. Soc. Jpn.* **1992**, *65*, 198−202.
(10) Imamura, T.; Sumiyoshi, T.; Takahashi, K.; Sasaki, Y. *J. Phys. Chem.* **1993**, *97*, 7786−7791.
(11) Abe, M.; Sasaki, Y.; Nagasawa, A.; Ito, T. *Bull. Chem. Soc. Jpn.* **1992**, *65*, 1411−1414.
(12) Abe, M.; Sasaki, Y.; Yamaguchi, T.; Ito, T. *Bull. Chem. Soc. Jpn.* **1992**, *65*, 1585−1590.
(13) Powell, G.; Richens, D. T.; Powell, A. K. *Inorg. Chim. Acta* **1993**, *213*, 147−155.
(14) Akashi, D.; Kido, H.; Sasaki, Y.; Ito, T. *Chem. Lett.* **1992**, 143−146.
(15) Cosnier, S.; Deronzier, A.; Llobet, A. *J. Electroanal. Chem.* **1990**, *280*, 213.
(16) (a) Ohto, A; Sasaki, Y.; Ito, T. *Inorg. Chem.* **1994**, *33*, 1245−1246. (b) Kobayashi, H.; Uryû, N.; Mogi, I.; Miyamoto, R.; Ohba, Y.; Iwaizumi, M.; Sasaki, Y.; Ohto, A.; Ito, T. *Bull. Chem. Soc. Jpn.* **1995**, *68*, 2551−2558. (c) Don, T.-Y.; Lee, H.-S.; Lee, T.-Y.; Hsieh, C.-F. *J. Chin. Chem. Soc.* (*Taipei*) **1992**, *39*, 393−399.
(17) Sasaki, Y.; Yoshida, Y.; Ohto, A.; Tokiwa, A.; Ito, T.; Kobayashi, H.; Uryû, N.; Mogi, I. *Chem. Lett.* **1993**, 69−72.
(18) Sasaki, Y.; Tokiwa, A.; Ito, T. *J. Am. Chem. Soc.* **1987**, *109*, 6341−6347.
(19) Sasaki, Y.; Nagasawa, A.; Tokiwa-Yamamoto, A.; Ito, T. *Inorg. Chim. Acta* **1993**, *212*, 175−182.

S0020-1669(96)00430-2 CCC: $12.00

multielectron redox catalysts. Synthetic examples of ligand-bridged Ru_3 clusters include the pyrazine-bridged dimer,[20] trimer,[21] and linear and branched tetramers[22] of the Ru_3 unit and Ru_3 complexes having bridged-metal complex fragments at terminal positions.[23] While a number of metal clusters involving redox-active metal centers and/or ligands have been described so far,[24−26] a detailed understanding of factors controlling the redox interactions between redox sites remains obscure because of the difficult preparation of cluster compounds in which both ligand and metal ion characteristics are systematically varied.

We previously introduced three redox-active *N*-methyl-4,4′-bipyridinium ions ($mbpy^+$) to the oxo-centered trinuclear cores and isolated $[M_3(\mu_3\text{-}O)(\mu\text{-}CH_3CO_2)_6(mbpy^+)_3]^{n+}$ ($M_3 = Ru_3$, Ru_2Rh, and Rh_3).[27] It was shown that the Ru_3 and Ru_2Rh complexes exhibit reversible multistep redox processes involving up to 11 electrons, based on redox of both trinuclear core and terminal ligands. Interestingly, three $mbpy^+$ ligands were reduced at different potentials with respect to the kind of metal ions involved: two-split waves (2e/1e ratio) for the Ru_3 complex, three-split waves (1e/1e/1e ratio) for the Ru_2Rh complex, and a single wave (3e) for the Rh_3 complex. This variation was accounted for by terminal ligand−ligand electronic interactions occurring through the $d\pi(Ru)-p\pi(\mu_3\text{-}O)$ molecular orbitals of the cluster core. Thus, tuning of ligand−ligand interactions can be achieved by modifing metal ions.

To obtain further insight into terminal ligand−ligand ($mbpy^+$) interactions in the triruthenium complexes, six mixed-terminal−ligand Ru_3 complexes are newly prepared in this study. The Ru_3 complexes investigated include $[Ru^{III}_2Ru^{II}(\mu_3\text{-}O)(\mu\text{-}CH_3CO_2)_6(mbpy^+)_2(CO)]^{2+}$ and $[Ru^{III}_3(\mu_3\text{-}O)(\mu\text{-}CH_3CO_2)_6(mbpy^+)_2(L)]^{3+}$, where L = H_2O, pyrazine (pz), pyridine (py), imidazole (Him), and 4-(dimethylamino)pyridine (dmap).[28] The complexes are schematically shown in Chart 1. The ligand−ligand interactions are discussed in terms of the extent of splitting of the ligand-based redox potentials in the cyclic and differential-pulse voltammograms. The X-ray crystal structure of the CO complex $[Ru^{III}_2Ru^{II}(\mu_3\text{-}O)(\mu\text{-}CH_3CO_2)_6(mbpy^+)_2(CO)](ClO_4)_2\cdot$2DMF (**1b**·2DMF) is also described as the first example of the valence-trapped $Ru^{III}_2Ru^{II}$ complex among the oxo-centered triruthenium analogs.

Chart 1

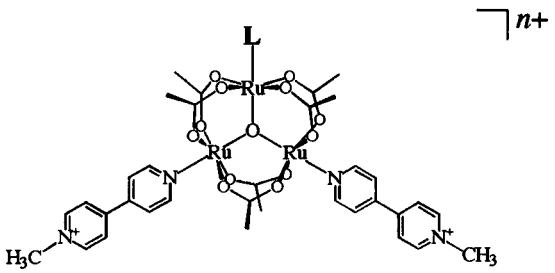

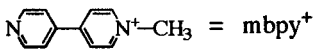

	PF_6^- salt	ClO_4^- salt
$[Ru^{III}_2Ru^{II}(O)(CH_3CO_2)_6(mbpy^+)_2(CO)]^{2+}$	**1a**	**1b**
$[Ru^{III}_3(O)(CH_3CO_2)_6(mbpy^+)_2(H_2O)]^{3+}$	**2a**	
$[Ru^{III}_3(O)(CH_3CO_2)_6(mbpy^+)_2(pz)]^{3+}$	**3a**	
$[Ru^{III}_3(O)(CH_3CO_2)_6(mbpy^+)_2(py)]^{3+}$	**4a**	**4b**
$[Ru^{III}_3(O)(CH_3CO_2)_6(mbpy^+)_2(Him)]^{3+}$	**5a**	
$[Ru^{III}_3(O)(CH_3CO_2)_6(mbpy^+)_2(dmap)]^{3+}$	**6a**	**6b**

(pz = pyrazine, py = pyridine, Him = imidazole, dmap = (4-dimethylamino)pyridine)

Experimental Section

1. Preparation. The ligand $[mbpy^+]PF_6$ was prepared according to the reported method[29] with slight modifications. $[Ru_3(O)(CH_3CO_2)_6(mbpy^+)_3](PF_6)_3$,[27] $[Ru_3(O)(CH_3CO_2)_6(H_2O)_2(CO)]\cdot H_2O$,[30] $[Ru_3(O)(CH_3CO_2)_6(py)_2(CO)]$,[4] and $[Ru_3(O)(CH_3CO_2)_6(pz)_2(CO)]\cdot 0.5pz$[21] were isolated according to the reported methods.

$[Ru_3(O)(CH_3CO_2)_6(mbpy^+)_2(CO)](PF_6)_2$ (1a). The CO complexes were prepared by two methods, both of which are analogous to those for the pyridine derivative $[Ru_3(O)(CH_3CO_2)_6(py)_2(CO)]$.[4]

Method 1. To a CH_3OH solution (30 cm^3) of $[Ru_3(O)(CH_3CO_2)_6(H_2O)_2(CO)]\cdot H_2O$ (603 mg, 0.798 mmol) was added $[mbpy^+]PF_6$ (640 mg, 2.02 mmol) at room temperature, and the mixture was refluxed for 15 min. Upon cooling, the volume of the resulting solution was reduced *in vacuo* to give dark blue solids. These were subjected to column chromatography with Sephadex LH-20 resin using acetone as eluent. A dark blue band was collected and evaporated to dryness. Nearly black crystals of **1a** were obtained from recrystallization from acetone/*n*-hexane (1/1, v/v) at room temperature and subsequent drying *in vacuo*. Yield: 560 mg (48%).

Method 2. $[Ru_3(O)(CH_3CO_2)_6(mbpy^+)_3](PF_6)_3\cdot 2H_2O$[27] (150 mg, 0.091 mmol) was dissolved in a CH_3CN/C_6H_6 (1/2, v/v, 30 cm^3) mixture. After the solution was degassed by N_2, CO was passed through the solution for 2 h at refluxing temperature, whereupon the color changed from deep purple to dark blue. The resulting solution was cooled with continuing CO bubbling. Dark blue solid **1a** was

(20) $[\{(py)_2Ru_3(O)(CH_3CO_2)_6\}_2(\mu\text{-}pz)](PF_6)_2$: (a) Baumann, J. A.; Salmon, D. J.; Wilson, S. T.; Meyer, T. J. *Inorg. Chem.* **1979**, *18*, 2472−2479. (b) Wilson, S. T.; Bondurant, R. F.; Meyer, T. J.; Salmon, D. J. *J. Am. Chem. Soc.* **1975**, *97*, 2285−2287.

(21) $[\{(py)_2Ru_3(O)(CH_3CO_2)_6(\mu\text{-}pz)\}_2\{(CO)Ru_2(O)(CH_3CO_2)_6\}](PF_6)_2$: Baumann, J. A.; Wilson, S. T.; Salmon, D. J.; Hood, P. L.; Meyer, T. J. *J. Am. Chem. Soc.* **1979**, *101*, 2916−2920.

(22) Ito, T.; Nagino, H.; Noguchi, Y.; Kido, H. International Chemical Congress of Pacific Basan Societies, Honolulu, Dec 1995; Abstract 698.

(23) (a) $[Ru_3(O)(CH_3CO_2)_6\{(\mu\text{-}pz)Fe(CN)_5\}_3]^{n-}$: Toma, H. E.; Matsumoto, F. M.; Cipriano, C. *J. Electroanal. Chem.* **1993**, *346*, 261−270. (b) $[Ru_3(O)(CH_3CO_2)_6\{(\mu\text{-}ampz)Ru(edta)\}_3]$ (ampz = 2-aminopyrazine, edta = ethylenediaminetetraacetate(2−)): Toma, H. E.; Olive, M. A. L. *Polyhedron* **1994**, *13*, 2647−2652.

(24) (a) Denti, G.; Serroni, S.; Campagna, S.; Juris, A.; Ciano, M.; Balzani, V. In *Perspectives in Coordination Chemistry*; Williams, A. F., Floriani, C., Merbach, A. S., Eds.; Verlag Helvetica Chimica Acta: Basel, Switzerland, 1992; pp 153−164. (b) Campagna, S.; Denti, G.; Serroni, S.; Juris, A.; Venturi, M.; Ricevuto, V.; Balzani, V. *Chem. Eur. J.* **1995**, *1*, 211−221.

(25) (a) Krejčík, M.; Vlček, A. A. *Inorg. Chem.* **1992**, *31*, 2390−2395. (b) Haga, M.; Bond, A. M. *Inorg. Chem.* **1991**, *30*, 475−480. (c) Haga, M.; Ano, T.; Kano, K.; Yamabe, S. *Inorg. Chem.* **1991**, *30*, 3843−3849.

(26) (a) Wheeler, B. L.; Nagasubramanian, G.; Bard, A. J.; Schechtman, L. A.; Dininny, D. R.; Kenny, M. E. *J. Am. Chem. Soc.* **1984**, *106*, 7404−7410. (b) Nevin, W. A.; Hempstead, M. R.; Liu, W.; Leznoff, C. C.; Lever, A. B. P. *Inorg. Chem.* **1987**, *26*, 570−577. (c) Kobayashi, N.; Lam, H.; Nevin, W. A.; Janda, P.; Leznoff, C. C.; Lever, A. B. P. *Inorg. Chem.* **1990**, *29*, 3415−3425.

(27) Abe, M.; Sasaki, Y.; Yamada, Y.; Tsukahara, K.; Yano, S.; Ito, T. *Inorg. Chem.* **1995**, *34*, 4490−4498.

(28) pK_a value of L.: pz, 0.6; py, 5.2; Him, 7.0; dmap, 9.7.

(29) Leopold, K. R.; Haim, A. *Inorg. Chem.* **1978**, *17*, 1753−1757.

(30) Although we adopted the preparative method reported for the bis(methanol)carbonyl complex $[Ru_3(O)(CH_3CO_2)_6(CH_3OH)_2(CO)]$[21] the product obtained here turned out to be a bis(aqua)carbonyl complex, $[Ru_3(O)(CH_3CO_2)_6(H_2O)_2(CO)]\cdot H_2O$. Anal. Calcd for $C_{13}H_{24}O_{17}Ru_3$: C, 20.66; H, 3.21. Found: C, 20.49; H, 3.16. IR (KBr pellet, cm^{-1}): ν(CO) = 1960 (s), ν_{asym}(OCO) = 1605 (s), 1570 (m), ν_{sym}(OCO) = 1425 (s). ^1H NMR (D_2O, *vs* TSP): δ 1.96 (12H, s, CH_3-acetate), 1.78 (6H, s, CH_3-acetate). See also Nagase, K.; Yokobayashi, H.; Watanabe, A.; Ishikawa, H.; Matsumoto T.; Kido, H.; Ito, T. *Netsu Sokutei* **1993**, *20*, 66−71.

precipitated by adding diethyl ether (20 cm^3) while stirring the solution at room temperature. The solid was collected by filtration and dried *in vacuo* (130 mg). The product was further purified and recrystallized similarly as in method 1. Yield: 86 mg (64%). Anal. Calcd for $[Ru_3(O)(CH_3CO_2)_6(mbpy^+)_2(CO)](PF_6)_2\cdot 2(CH_3)_2CO\cdot H_2O$ ($C_{41}H_{54}O_{17}N_4P_2F_{12}Ru_3$): C, 33.54; H, 3.72; N, 3.82. Found: C, 33.32; H, 3.72; N, 3.84. IR (cm^{-1}, KBr pellet, 2000−1300 cm^{-1} region): 1940 (s, ν(CO)), 1655 (m), 1610 (s, ν_{asym}(OCO)), 1570 (m, ν_{asym}(OCO)), 1560 (m), 1500 (m), 1422 (s, ν_{sym}(OCO)), 1355 (m), 1340 (w).

$[Ru_3(O)(CH_3CO_2)_6(mbpy^+)_2(CO)](ClO_4)_2\cdot 2C_6H_5CH_3$ (1b·2$C_6H_5CH_3$). A PF_6^- salt of **1a** (100 mg, 0.068 mmol) was dissolved in CH_3CN (3 cm^3), and a solid $NaClO_4$ (84 mg, 0.686 mmol) was added. The mixture was stirrred until the $NaClO_4$ was dissolved, and it was filtered. To the filtrate was added toluene (4 cm^3), and this mixture was kept at room temperature overnight. The blackish blue crystals appeared and were collected by filtration and dried *in vacuo*. Yield: 58 mg (60%). The existence of two toluene solvates per one molecule was confirmed by the ^1H NMR spectrum in CD_3CN. ^1H NMR (CD_3CN, *vs* TMS): δ 9.39 (4H, d, mbpy$^+$), 9.05 (4H, d, mbpy$^+$), 8.71 (4H, d, mbpy$^+$), 8.64 (4H, d, mbpy$^+$), 4.65 (6H, s, CH_3−mbpy$^+$), 2.09 (12H, s, CH_3-acetate bridging (CO)Ru···Ru(mbpy$^+$)), 2.07 (6H, s, CH_3-acetate bridging (mbpy$^+$)Ru···Ru(mbpy$^+$)). The solid-state structure of the toluene-solvated complex was also confirmed by X-ray analysis.[31]

$[Ru_3(O)(CH_3CO_2)_6(mbpy^+)_2(CO)](ClO_4)_2\cdot 2DMF$ (1b·2DMF). Slow recrystallization (ca. 1 month) of **1b**·2$C_6H_5CH_3$ from DMF/diethyl ether under Ar at room temperature gave a DMF-solvated complex, $[Ru_3(O)(CH_3CO_2)_6(mbpy^+)_2(CO)](ClO_4)_2\cdot 2DMF$ (**1b**·2DMF), which was structurally characterized by X-ray crystallography.

$[Ru_3(O)(CH_3CO_2)_6(mbpy^+)_2(CO)]\{B(C_6H_5)_4\}_2$ (1c). A $B(C_6H_5)_4^-$ salt, **1c**, was precipitated by adding an excess of $NaB(C_6H_5)_4$ to an aqueous solution of **1a**. The solid was collected by filtration and dried *in vacuo*. ^1H NMR (CD_3CN) δ 9.26 (4H, d, mbpy), 8.78 (4H, d, mbpy), 8.50 (4H + 4H, d, mbpy), 4.39 (6H, s, CH_3-mbpy$^+$), 2.05 (12H, s, CH_3-acetate bridging (CO)Ru···Ru(mbpy$^+$)), 1.85 (6H, s, CH_3-acetate bridging (mbpy$^+$)Ru···Ru(mbpy$^+$)). Signals from $B(C_6H_5)_4^-$ were observed at δ 7.28 (16H, s), 6.99 (16H, t), and 6.86 (8H, t).

$[Ru_3(O)(CH_3CO_2)_6(mbpy^+)_2(H_2O)](PF_6)_3$ (2a). A suspension of **1a** (460 mg, 0.33 mmol) in CH_3OH (3 cm^3) was stirred for 30 min and was filtered. To the filtrate was added a 10% Br_2/CH_3OH solution with stirring, whereupon the color immediately changed from dark blue to green. NH_4PF_6 (114 mg, 0.70 mmol) dissolved in CH_3OH (2 cm^3) was added to the solution which was stirred for 10 min and evaporated to dryness by rotary evaporator. Green microcrystalline solid of **2a** was obtained from recrystallization of the residue from CH_3OH/diethyl ether at 0 °C. Yield: 222 mg (44%). Anal. Calcd for $[Ru_3(O)(CH_3CO_2)_6(mbpy^+)_2(H_2O)](PF_6)_3\cdot H_2O$ ($C_{34}H_{44}O_{15}N_4P_3F_{18}Ru_3$): C, 27.20; H, 2.96; N, 3.73. Found: C, 27.67; H, 3.05; N, 3.68. IR (cm^{-1}, KBr pellet, 1700−1300 cm^{-1} region): 1650 (m), 1620 (m), 1550 (m), 1500 (m), 1430 (s, ν_{sym}(OCO)), 1355 (w), 1330 (w).

$[Ru_3(O)(CH_3CO_2)_6(mbpy^+)_2(pz)](PF_6)_3$ (3a). To a CH_3OH solution of **2a** was added pyrazine (70 mg, 1.8 mmol), and the mixture was kept at 40 °C for 24 h with stirring. The resultant solution was evaporated to dryness by rotary evaporator, and the residue was dissolved in a minimal amount of CH_3CN. This was treated with column chromatography using a Sephadex LH-20 resin with CH_3CN/CH_3OH (1/9, v/v) as eluent. The main fraction was collected, and NH_4PF_6 was added. The mixture was stirred for several minutes, and the solvent was evaporated *in vacuo*. The crystalline solid of **3a** was obtained by recrystallization of the residue from CH_3CN/diethyl ether at 0 °C. Yield: 30 mg (59%). Anal. Calcd for $[Ru_3(O)(CH_3CO_2)_6(mbpy^+)_2(pz)](PF_6)_3\cdot H_2O$ ($C_{38}H_{46}O_{14}N_6P_3F_{18}Ru_3$): C, 29.46; H, 3.00; N, 5.43. Found: C, 29.81; H, 2.90; N, 5.49. IR (cm^{-1}, KBr pellet, 1700−1300 cm^{-1} region): 1645 (m), 1620 (m), 1590 (m), 1545 (m), 1530 (m), 1500 (m), 1425 (s, ν_{sym}(OCO)), 1355 (m), 1330 (w).

$[Ru_3(O)(CH_3CO_2)_6(mbpy^+)_2(py)](X)_3$ (X = PF_6^- (4a), ClO_4^- (4b)). To a CH_3OH solution (100 cm^3) of **2a** (100 mg, 0.067 mmol) was added pyridine (0.2 cm^3, 2.53 mmol), and the solution was stirred for 5 h at room temperature, during which the crude product of **4a** was precipitated. The precipitates were collected and purified by column chromatography (Sephadex LH-20 resin with ethanol as eluent). NH_4PF_6 was added to the main fraction, and the mixture was evaporated to dryness. The residue was recrystallized from acetone/diethyl ether (1/2, v/v), which gave crystalline solids of **4a**. Yield: 73 mg (70%). Anal. Calcd for $[Ru_3(O)(CH_3CO_2)_6(mbpy^+)_2(py)](PF_6)_3\cdot 2H_2O$ ($C_{39}H_{49}O_{15}N_5P_3F_{18}Ru_3$): C, 29.91; H, 3.16; N, 4.47. Found: C, 29.68; H, 3.12; N, 4.69. The perchlorate salt **4b** was obtained by adding solid $NaClO_4$ to the eluent instead of NH_4PF_6. Anal. Calcd for $[Ru_3(O)(CH_3CO_2)_6(mbpy^+)_2(py)](ClO_4)_3\cdot NaClO_4$ ($C_{39}H_{45}O_{29}N_5NaCl_4Ru_3$): C, 30.89; H, 3.00; N, 4.62. Found: C, 31.04; H, 3.08; N, 4.46. IR (cm^{-1}, KBr pellet, 1700−1300 cm^{-1} region): 1640 (m), 1615 (m), 1590 (m), 1540 (m), 1495 (m), 1420 (s, ν_{sym}(OCO)), 1350 (m), 1325 (w).

$[Ru_3(O)(CH_3CO_2)_6(mbpy^+)_2(Him)](PF_6)_3$ (5a). To a CH_3CN solution (30 cm^3) of **2a** (170 mg, 0.12 mmol) was added solid imidazole (400 mg, 5.9 mmol), and the mixture was allowed to react for 12 h at room temperature. The resultant solution was evaporated to dryness and the residue was dissolved in a minimal amount of acetone (ca. 2 cm^3), which was treated with the column of LH-20 resin. The column was first washed with acetone, and then the products were eluted with CH_3OH/acetone (1/9, v/v). The green fraction was collected and evaporated to dryness. The crystalline solid **5a** was obtained by recrystallization of the residue from CH_3OH (10 cm^3) containing NH_4PF_6 (100 mg). Yield: 59 mg (34%). Anal. Calcd for $[Ru_3(O)(CH_3CO_2)_6(mbpy^+)_2(Him)](PF_6)_3\cdot 2H_2O$ ($C_{37}H_{48}O_{15}N_6P_3F_{18}Ru_3$): C, 28.67; H, 3.13; N, 5.42. Found: C, 28.71; H, 3.27; N, 5.42. IR (cm^{-1}, KBr pellet, 1700−1300 cm^{-1} region): 1640 (m), 1620 (m), 1580 (m), 1545 (m), 1530 (m), 1500 (m), 1430 (s, ν_{sym}(OCO)), 1355 (m), 1330 (w).

$[Ru_3(O)(CH_3CO_2)_6(mbpy^+)_2(dmap)](X)_3$ (X = PF_6^- (6a), ClO_4^- (6b)). To a CH_3CN solution (30 cm^3) of **2a** (100 mg, 0.068 mmol) was added 4-(dimethylamino)pyridine (416 mg, 0.034 mmol), and the mixture was allowed to react for 12 h at room temperature. Then the solvent was evaporated to dryness. The residue was washed with a copious amount of acetone and diethyl ether, and the residue was dissolved in CH_3OH. An addition of diethyl ether afforded a crude product of **6a**. The perchlorate salt **6b** was obtained by recrystallization of the PF_6^- salt **6a** from CH_3CN/diethyl ether mixture containing an excess amount of $NaClO_4$. Anal. Calcd for $[Ru_3(O)(CH_3CO_2)_6(mbpy^+)_2(dmap)](ClO_4)_3\cdot 0.5NaClO_4\cdot 2H_2O$ ($C_{41}H_{54}O_{29}N_6Na_{0.5}Cl_{3.5}Ru_3$): C, 32.10; H, 3.56; N, 5.48. Found: C, 32.31; H, 3.61; N, 5.33. IR (cm^{-1}, KBr pellet, 1700−1300 cm^{-1} region): 1640 (m, sh), 1620 (s), 1580 (m), 1540 (s), 1495 (m), 1420 (s, ν_{sym}(OCO)), 1350 (m), 1330 (w).

Caution! Perchlorate salts of metal complexes with organic ligands are potentially explosive. The materials should be handled with extreme care in small quantities.

2. Materials. CH_3CN used in electrochemical measurements was distilled twice over P_2O_5 and then once over CaH_2 under a nitrogen atmosphere before use. Tetra-*n*-butylammonium hexafluorophosphate $[(n\text{-}C_4H_9)_4N]PF_6$ was prepared by mixing an aqueous solution of $[(n\text{-}C_4H_9)_4N]Br$ with that of NH_4PF_6 and was recrystallized three times from hot ethyl acetate/benzene and dried *in vacuo* at 140 °C. $RuCl_3\cdot nH_2O$ (Wako Pure Chemicals) and other reagents were used as received.

3. Measurements. Electronic absorption spectra were recorded on Hitachi 330 and 340 spectrophotometers. ^1H NMR spectra were obtained on a JEOL GSX-270 FT NMR spectrometer at 270 MHz. Chemical shifts are reported with respect to an internal reference of TMS for CD_3CN solution and of TSP for D_2O solution. Infrared

(31) The solid-state structure of this complex was confirmed to be identical to that in **1b**·2DMF described below. However, due to the poor quality of the crystal and severe disorder of the toluene molecules, the result is insufficient and is not discussed here in detail. The crystal used for the crystallographic analysis was obtained as described in the Experimental Section. The crystal data were collected at 25 °C on a Rigaku AFC-7S diffractometer with graphite-monochromated Mo Kα (λ = 0.710 73 Å) radiation. **1b**·2$C_6H_5CH_3$ crystallizes in the monoclinic space group *C*2/*c* (No. 15) with cell constants of a = 35.763(4) Å, b = 11.442(5) Å, c = 15.486(5) Å, β = 114.02(1)°, V = 5788(2) Å^3, Z = 4, d_{calcd} = 1.638 g cm^{-1}, and R = 0.082 (R_w = 0.106) for 4555 independent reflections. Important interatomic distances and angles of **1b**·2$C_6H_5CH_3$ are as follows: (CO)Ru···Ru(mbpy$^+$) = 3.414(2) Å, (mbpy$^+$)Ru···Ru(mbpy$^+$) = 3.293(2) Å, (CO)Ru−(μ_3-O) = 2.07(2) Å, (mbpy$^+$)Ru−(μ_3-O) = 1.888(7) Å, (mbpy$^+$)Ru−N = 2.13(1) Å, (CO)Ru−(μ_3-O)−Ru(mbpy$^+$) = 119.3(4)°, and (mbpy$^+$)-Ru−(μ_3-O)−Ru(mbpy$^+$) = 121.4(8)°.

Table 1. Crystallographic Data for $[Ru^{III}_2Ru^{II}(\mu_3\text{-}O)(\mu\text{-}CH_3CO_2)_6(mbpy^+)_2(CO)](ClO_4)_2\cdot 2DMF$ (**1b**·2DMF)

formula	$C_{41}Cl_2H_{54}N_6O_{24}Ru_3$
fw	1389.12
cryst sysr	monoclinic
space group	$P2_1/m$ (No. 11)
radiation	Mo Kα (λ = 0.710 73 Å)
temperature, K	298
a, Å	8.740(6)
b, Å	32.269(6)
c, Å	10.276(4)
β, deg	103.37(5)
V, Å^3	2820(2)
Z	2
d_{calcd}, g cm^{-3}	1.636
μ(Mo Kα), cm^{-1}	9.557
2θ, deg	$3 < 2\theta < 55$
no. of reflcns measd	5621
no. of indep reflcns	5277 ($\|F_o\| > 3\sigma(\|F_o\|)$)
no. of reflcns used for calcn	2242
R^a/R_w^b	0.071/0.074

[a] $R = \sum||F_o| - |F_c||/\sum|F_o|$. [b] $R_w = [\sum w(|F_o| - |F_c|)^2)/\sum w|F_o|^2]^{1/2}$; $w^{-1} = \sigma(F_o)^2 + (0.020F_o)^2$.

absorption spectra were recorded with KBr pellets on a Jasco IR-810 spectrophotometer.

Cyclic voltammetry (CV) and differential-pulse voltammetry (DPV) were carried out by using a YANACO P-1100 polarographic analyzer with a WATANABE WX 1100 X-Y recorder. A three-electrode cell consisting of a glassy carbon working electrode, a platinum wire counter electrode, and an Ag/Ag^+ ($[AgClO_4] = 0.01$ M in CH_3CN) reference electrode was used. CV was performed at scan rates of 5−500 mV s^{-1}. The half-wave potentials $E_{1/2} = (E_{pc} + E_{pa})/2$, where E_{pc} and E_{pa} are the cathodic and anodic peak potential, respectively, are given at a scan rate of 100 mV s^{-1}. Under these experimental conditions, a one-electron reversible wave of ferrocene (1 mM) was detected at $E_{1/2}$ = +0.09 V *vs* Ag/Ag^+ with ΔE_p (= $E_{pa} - E_{pc}$) = 60 mV. All the potentials are reported with respect to the Fc/Fc^+ couple in this study. DPV was performed at a scan rate of 20 mV s^{-1} with pulse height of 5 mV. Controlled-potential absorption spectra were obtained with an optically transparent thin-layer electrode (OTTLE) cell. The working and the counter electrodes were gold mesh, and the potential was referred to an Ag/AgCl reference electrode. The spectra were measured with a Shimazu UV-2100 spectrophotometer. All electrochemical and spectroelectrochemical measurements were carried out under a nitrogen atmosphere.

4. X-ray Crystallography. Single crystals of $[Ru_3(O)(CH_3CO_2)_6(mbpy^+)_2(CO)](ClO_4)_2\cdot 2DMF$ (**1b**·2DMF) suitable for X-ray crystallography were obtained by slow recrystallization of **1b**·$2C_6H_5CH_3$ in a mixed DMF/diethyl ether solution at room temperature. A dark blue prismatic crystal of **1b**·2DMF was attached on top of a glass fiber and coated with an epoxy resin, and it was mounted on a Rigaku AFC-5R diffractometer with graphite-monochromated Mo Kα (λ = 0.710 73 Å) radiation. The X-ray data were collected at 25 °C. The ω scan technique was employed. The lattice constants were determined by a least-squares refinement using automatically centered 25 reflections in the range $25° < 2\theta < 30°$. Three standard reflections were measured every 150 reflections, and they showed no sign of appreciable decay throughout the data collection. The structure was solved by a direct method using the SHELXS-86 program.[32] All non-hydrogen atoms were located by Fourier synthesis and full-matrix least-squares and refined anisotropically. Hydrogen atoms were located by calculation only for those bonded to aromatic carbon atoms of $mbpy^+$ ligands and were refined isotropically. Absorption correction was made by an empirical method based on a set of ψ scans.[33] Crystallographic and other experimental data are listed in Table 1. All of the calculations were performed on a Fujitsu S-4/IX workstation using Xtal 3.2 program packages.[34]

Results

1. Synthesis and Characterizations. Triruthenium complexes with mixed-terminal ligands, $[Ru_3(\mu_3\text{-}O)(\mu\text{-}CH_3CO_2)_6(mbpy^+)_2(CO)]^{2+}$ and $[Ru_3(\mu_3\text{-}O)(\mu\text{-}CH_3CO_2)_6(mbpy^+)_2(L)]^{3+}$ (L = H_2O, pz, py, Him, and dmap), were prepared by analogous synthetic procedures to those reported for $[Ru_3(\mu_3\text{-}O)(\mu\text{-}CH_3CO_2)_6(py)_2(CO)]$ and $[Ru_3(\mu_3\text{-}O)(\mu\text{-}CH_3CO_2)_6(py)_2(pz)]PF_6$,[4] respectively.

The PF_6^- salt of the CO complex **1a** was isolated by two independent methods (eqs 1 and 2). The CO complexes were

$$[Ru_3(O)(CH_3CO_2)_6(mbpy^+)_3](PF_6)_3 + CO \rightarrow [Ru_3(O)(CH_3CO_2)_6(mbpy^+)_2(CO)](PF_6)_2 + [mbpy^+]PF_6 \quad (1)$$

$$[Ru_3(O)(CH_3CO_2)_6(H_2O)_2(CO)] + 2[mbpy^+]PF_6 \rightarrow [Ru_3(O)(CH_3CO_2)_6(mbpy^+)_2(CO)](PF_6)_2 + 2H_2O \quad (2)$$

isolated as PF_6^-, ClO_4^-, and $B(C_6H_5)_4^-$ salts. Complex **1a** was characterized by a strong IR band of ν(CO) (1940 cm^{-1}) and its diamagnetic ^1H NMR spectrum. The solid-state structure of the perchlorate salt **1b**·2DMF was also confirmed by X-ray crystallography (see below).

Bromine oxidation of **1a** in a moist CH_3OH solution at room temperature gave aqua complex **2a**. Facile ligand-substitution reaction of the coordinated water in **2a** by an excess L (pz, py, Him, and dmap) in CH_3OH solution was observed, leading to the isolation of the L-coordinated mixed-ligand complexes (eq 3).

$$[Ru_3(O)(CH_3CO_2)_6(mbpy^+)_2(H_2O)](PF_6)_3 + L \rightarrow [Ru_3(O)(CH_3CO_2)_6(mbpy^+)_2(L)](PF_6)_3 + H_2O \quad (3)$$

On the basis of the visible absorption spectral change, the reaction completed within ca. 20 h for L = pz (40 °C) and ca. 12 h for L = dmap (25 °C). These reactions thus took place only at the Ru site with an aqua ligand but not at two Ru sites with $mbpy^+$ ligands. The mixed-terminal ligand tririutheium complexes thus obtained were isolated in the Ru^{III}_3 oxidation state as PF_6^- and/or ClO_4^- salts.

Infrared spectra of the present triruthenium complexes show an intense symmetric stretching band of bridging acetate in the 1420−1430 cm^{-1} region. Asymmetric stretching bands are detected as two strong absorptions at 1605 and 1570 cm^{-1} for **1a**; however, for other triruthenium(III) complexes **2a**−**6b**, the corresponding band is observed to be less intense[35] or masked by absorptions due to $mbpy^+$ ligands.

2. X-ray Structure of $[Ru_3(\mu_3\text{-}O)(\mu\text{-}CH_3CO_2)_6(mbpy^+)_2(CO)](ClO_4)_2\cdot 2DMF$. The solid-state structure of the CO complex $[Ru_3(\mu_3\text{-}O)(\mu\text{-}CH_3CO_2)_6(mbpy^+)_2(CO)](ClO_4)_2\cdot 2DMF$ (**1b**·2DMF) was unambiguously determined by X-ray crystallography. The ORTEP drawing of the cationic portion of **1b**·2DMF is shown in Figure 1, part a. The trinuclear core framework is displayed in Figure 1, part b, together with important interatomic distances. Final atomic positional and thermal parameters for non-hydrogen atoms are shown in Table

(32) Sheldrick, G. M. *SHELXS-86, Program for Crystal Structure Determination*; University of Göttingen: Germany, 1986.
(33) Watenpaugh, K; Stewart, J. *ABSCAL, Scale Diffractometer Intensity Data in Xtal 3.2 Program System.*
(34) Hall, S. R.; Flank, H. D.; Stewart, J. M. *Xtal 3.2, Program for Crystal Structure Analysis*; University of Western Australia: Geneva, Switzerland, and Maryland, 1992.
(35) Ohto, A.; Tokiwa-Yamamoto, A.; Abe, M.; Ito, T.; Sasaki, Y.; Umakoshi, K.; Cannon, R. D. *Chem. Lett.* **1995**, 97−98.

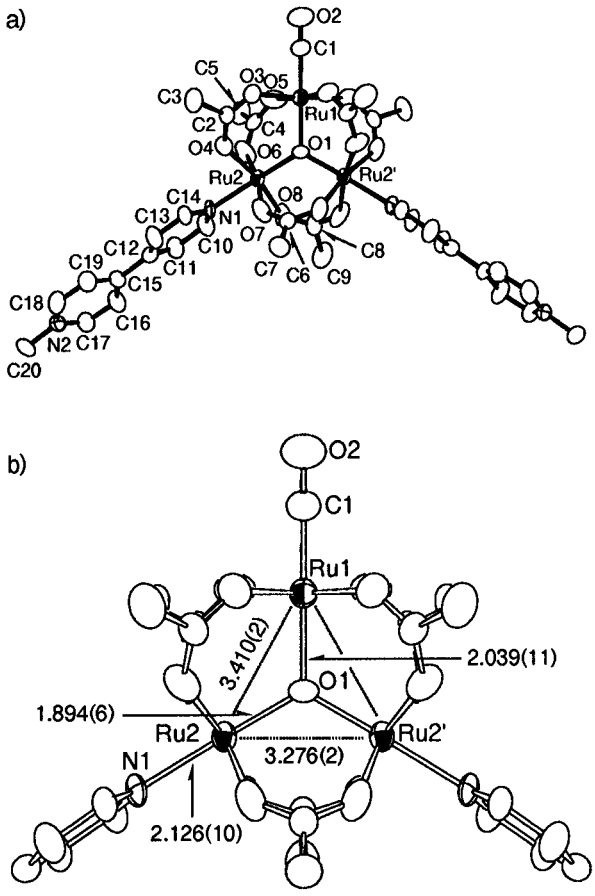

Figure 1. (a) ORTEP drawing of a cationic portion of $[Ru^{III}_2Ru^{II}(\mu_3\text{-}O)(\mu\text{-}CH_3CO_2)_6(mbpy^+)_2(CO)](ClO_4)_2\cdot 2DMF$ (**1b**·2DMF) with thermal ellipsoids of 50% probability level. Hydrogen atoms are omitted for clarity. (b) The trinuclear core structure in **1b**·2DMF with important intramolecular atomic distances (Å).

Table 2. Selected Interatomic Distances (Å) and Bond Angles (deg) for $[Ru^{III}_2Ru^{II}(\mu_3\text{-}O)(\mu\text{-}CH_3CO_2)_6(mbpy^+)_2(CO)](ClO_4)_2\cdot 2DMF$ (**1b**·2DMF)

Distances (Å)			
Ru1···Ru2	3.410(2)	Ru2−O6	2.023(11)
Ru2···Ru2′	3.276(2)	Ru2−O7	2.041(11)
Ru1−O1	2.039(11)	Ru2−O8	2.033(12)
Ru1−C1	1.839(20)	C1−O2	1.132(27)
Ru1−O3	2.062(12)	C4−O5	1.229(18)
Ru1−O5	2.074(12)	C4−O6	1.249(16)
Ru2−O1	1.894(6)	C4−C5	1.534(23)
Ru2−N1	2.126(10)	C12−C15	1.510(19)
Ru2−O4	2.030(11)	N2−C20	1.484(20)
Angles (deg)			
Ru1−O1−Ru2	120.2(3)	N1−Ru2−O4	86.1(4)
Ru2−O1−Ru2′	119.7(6)	N1−Ru2−O6	85.2(4)
O1−Ru1−C1	178.2(9)	N1−Ru2−O7	84.7(4)
Ru1−C1−O2	179(3)	N1−Ru2−O8	83.6(4)
C1−Ru1−O3	89.4(7)	Ru1−O5−C4	133(1)
C1−Ru1−O5	86.9(7)	O5−C4−O6	128(1)
O1−Ru2−N1	178.6(4)	Ru2−O6−C4	133(1)

S-2 (supporting information). Selected interatomic distances and bond angles are collected in Table 2.

The most prominent structural feature of **1b** is that three Ru ions form an isosceles triangle rather than an equilateral triangle. The Ru1···Ru2 distance (3.410(2) Å) is considerably longer than the Ru2···Ru2′ distance (3.276(2) Å). This difference is due to lengthening of the Ru1−O1 bond (2.039(11) Å) as compared with that of the Ru2−O1 bond (1.894(6) Å). The trinuclear core structure in **1b** is thus in a marked contrast to the previously characterized triruthenium complexes with three identical terminal ligands;[36] in these complexes, three Ru···Ru distances are the same or essentially the same irrespective of formal oxidation states of Ru atoms. Thus, these triruthenium complexes may have delocalized electronic states with an averaged ruthenium oxidation number. On the basis of such comparison, it is concluded that the triruthenium core in **1b** is in the valence-trapped state; namely, Ru1 bound with the CO ligand is in the divalent state, while Ru2 and Ru2′ bound with $mbpy^+$ ligands are in the trivalent state. The CO ligand stabilizes the +2 oxidation state of Ru1. It is also pointed out that the $Ru^{III}-(\mu_3\text{-}O)$ and $Ru^{II}-(\mu_3\text{-}O)$ distances in **1b** are much shorter and longer as compared to the averaged $Ru-(\mu_3\text{-}O)$ distance in $[Ru_3(\mu_3\text{-}O)(\mu\text{-}CH_3CO_2)_6\{P(C_6H_5)_3\}_3]$ (1.92 Å),[36a] which has formally the same oxidation state as **1b**. The $Ru-(\mu_3\text{-}O)$ distances of other Ru^{III}_3 and $Ru^{III}_2Ru^{IV}$ complexes have been reported to be 1.907(4)−1.935(2) Å.[36b−d] In spite of the clear differences between $Ru^{II}-(\mu_3\text{-}O)$ and $Ru^{III}-(\mu_3\text{-}O)$ bond lengths, $Ru^{II/III}-O$(acetate) distances do not seem to show a significant difference beyond the experimental error. The Ru2−N1 distance in **1b** (2.126(10) Å) is comparable to the $Ru^{III}-N$(py) distance found in $[Ru^{III}_3(O)(C_6H_5CO_2)_6(py)_3]PF_6$ (2.134(8) Å).[12]

3. ^{1}H NMR Spectroscopy. ^{1}H NMR data for the $mbpy^+$ complexes in CD_3CN at room temperature are collected in Table 3. Chemical shift data clearly show that the CO complex **1a** ($Ru^{III}_2Ru^{II}$) is diamagnetic, while complexes **2a**−**6b** (Ru^{III}_3) are paramagnetic. However, all of the signals for Ru^{III}_3 complexes are found in a rather narrow chemical shift range (δ 8.60 to −0.66) and appear to be still sharp.[4] These resonances can be assigned on the basis of their chemical shifts and the relative integrated intensity ratio. In addition, for the assignments of terminal ligand signals of Ru^{III}_3 complexes, larger paramagnetic shift is also assumed for protons closer toward Ru^{III} centers. The presence of two kinds of terminal ligands (two $mbpy^+$ and one L ligands) is clearly confirmed by two acetate methyl singlets in 2/1 integrated intensity ratio. For every Ru^{III}_3 complex, a methyl resonance of acetates bridging (L)Ru···Ru-($mbpy^+$) (12H) appears at lower field relative to that of acetates bridging ($mbpy^+$)Ru···Ru($mbpy^+$) (6H); e.g., δ 2.05 (12H) and 1.85 (6H) for **1a** and δ 5.29 (12H) and 5.05 (6H) for **2a**.

4. Absorption Spectroscopy. The present mixed-ligand triruthenium complexes show distinctive absorption spectral patterns in a UV−vis region, depending on both the Ru_3 oxidation states and the kind of terminal ligand L. The absorption bands for Ru^{III}_3 complexes **2a**−**6b** in CH_3CN are summarized in Table 4 and those for CO complex **1a** in Table 5. Table 5 also includes absorption data for the reference complexes $[Ru_3(O)(CH_3CO_2)_6(py)_2(CO)]$[4] and $[Ru_3(O)(CH_3CO_2)_6(pz)_2(CO)]\cdot 0.5pz$.[21] For Ru^{III}_3 complexes, band assignments were made on the basis of a previously described qualitative $d\pi(Ru)-p\pi(\mu_3\text{-}O)$ molecular orbital diagram for the $Ru_3(\mu_3\text{-}O)$ cluster in D_{3h} symmetry.[4,36a]

A broad band centered at 685−702 nm with a shoulder at 620−630 nm observed in Ru^{III}_3 complexes (band I) is assigned to transitions from occupied nonbonding orbitals to a vacant antibonding orbital arising from $d\pi(Ru)-p\pi(\mu_3\text{-}O)$ interactions (intracluster transitions). A band found at 380−422 nm (band II) is due to charge-transfer transitions from $d\pi-p\pi$ molecular

(36) Structurally characterized oxo-centered triruthenium complexes: (a) $[Ru^{III}_2Ru^{II}(O)(CH_3CO_2)_6\{P(C_6H_5)_3\}_3]$: Cotton, F. A.; Norman, J. G. Jr. *Inorg. Chim. Acta* **1972**, *6*, 411−419. (b) $[Ru^{III}_3(O)(C_6H_5CO_2)_6(py)_3]PF_6$, see ref 12. (c) $[Ru^{III}_3(O)(CH_3CO_2)_6(H_2O)_3]ClO_4\cdot 2H_2O$: Powell, G.; Richens, D. T.; Bino, A. *Inorg. Chim. Acta* **1995**, *232*, 167−170. (d) $[Ru^{III}_3(O)(CH_3CO_2)_6(H_2O)_3]BF_4\cdot 2H_2O$, $[Ru^{III}_3(O)(HCO_2)_6(H_2O)_3]BF_4\cdot 3H_2O$, and $[Ru^{III}_2Ru^{IV}(O)(CH_3CO_2)_6(H_2O)_3](ClO_4)_2\cdot H_2O$: Almog, O.; Bino, A.; Garfinkel-Shweky, D. *Inorg. Chim. Acta* **1993**, *213*, 99−102.

Table 3. ^{1}H NMR Data for the Triruthenium Complexes $[Ru_3(O)(CH_3CO_2)_6(mbpy^+)_2(CO)]^{2+}$ and $[Ru_3(O)(CH_3CO_2)_6(mbpy^+)_2(L)]^{3+}$ [a]

		mbpy$^+$						
complex	L	2′,6′-H	3′,5′-H	3,5-H	2,6-H	C*H*$_3$	C*H*$_3$-acetate	L
1a	CO	9.27 (4H, d)	8.86 (4H, d)	8.55 (4H + 4H, d)		4.44 (6H, s)	2.05 (12H, s) 1.85 (6H, s)	
2a	H_2O	8.35 (4H, d)	7.46 (4H, s)	6.48 (4H, s)	−0.66 (4H, s)	4.02 (6H, s)	5.29 (12H, s) 5.05 (6H, s)	
								(pz)
3a	pz	8.60 (4H, d)	7.75 (4H, d)	5.90 (4H, d)	0.79 (4H, d)	4.15 (6H, s)	5.55 (12H, s) 5.45 (6H, s)	0.70 (2H, s, 2,6-*H*) 2.11 (2H, s, 3,5-*H*)
								(py)
4b	py	8.45 (4H, d)	7.67 (4H, d)	5.94 (4H, d)	0.85 (4H, d)	4.11 (6H, s)	5.29 (12H, s) 5.04 (6H, s)	0.15 (2H, s, 2,6-*H*) 5.65 (2H, t, 3,5-*H*) 6.61 (1H, t, 4-*H*)
								(Him)
5a	Him	8.58 (4H, d)	7.71 (4H, d)	5.94 (4H, s)	0.39 (4H, s)	4.14 (6H, s)	4.62 (12H, s) 4.45 (6H, s)	10.80 (1H, s, 1-*H*) 3.04 (1H, s, 2- or 4-*H*) 2.31 (1H, s, 4- or 2-*H*) 6.18 (1H, s, 5-H)
								(dmap)
6b	dmap	8.46 (4H, d)	7.66 (4H, d)	5.92 (4H, s)	0.43 (4H, s)	4.11 (6H, s)	4.63 (12H, s) 4.29 (6H, s)	2.22 (2H, d, 2,6-*H*) 5.75 (2H, d, 3,5-*H*) 4.72 (6H, s, C*H*$_3$)

[a] Measured in CD_3CN at room temperature. Chemical shifts are reported *vs* TMS.

Table 4. Absorption Spectral Data for the Triruthenium Complexes $[Ru_3(O)(CH_3CO_2)_6(mbpy^+)_2(L)]^{3+}$ (L = H_2O, pz, py, Him, and dmap) in CH_3CN at Room Temperature

	λ_{max}, nm (ϵ, $M^{-1}\,cm^{-1}$)		
complex	band I[a]	band II[b]	band III[c]
$[Ru_3(O)(CH_3CO_2)_6(mbpy^+)_2(H_2O)](PF_6)_3$ (**2a**)	702 (6400), 630 sh	390 (8700)	255 (42 000)
$[Ru_3(O)(CH_3CO_2)_6(mbpy^+)_2(pz)](PF_6)_3$ (**3a**)	697 (7800), 630 sh	380 (11 800)	255 (51 900)
$[Ru_3(O)(CH_3CO_2)_6(mbpy^+)_2(py)](ClO_4)_3$ (**4b**)	700 (7200), 630 sh	395 (9100)	255 (47 400)
$[Ru_3(O)(CH_3CO_2)_6(mbpy^+)_2(Him)](PF_6)_3$ (**5a**)	692 (7000), 620 sh	398 (9100)	256 (50 800)
$[Ru_3(O)(CH_3CO_2)_6(mbpy^+)_2(dmap)](ClO_4)_3$ (**6b**)	685 (8000), 630 sh	422 (10 000)	260 (53 800)

[a] Transitions between molecular orbitals arising from dπ(Ru)−pπ(μ_3-O) interactions within the Ru_3(μ_3-O) core. [b] Charge-transfer transitions from dπ(Ru)−pπ(μ_3-O) orbitals of the Ru_3(μ_3-O) core to π^* orbitals of terminal ligands. [c] $\pi-\pi^*$ transitions in terminal ligands.

Table 5. Absorption Spectral Data for the Triruthenium Carbonyl Complexes $[Ru_3(O)(CH_3CO_2)_6(A)_2(CO)]^{n+}$ (A = py (n = 0), pz (n = 0), and mbpy$^+$ (n = 2)) at Room Temperature

		λ_{max}, nm (ϵ/$M^{-1}\,cm^{-1}$)		
complex	solvent	band I[a]	band II[b]	band III[c]
$[Ru_3(O)(CH_3CO_2)_6(py)_2(CO)]$[d]	CH_3CN	580 (4500)	333 (6200)	250 (15 900)
$[Ru_3(O)(CH_3CO_2)_6(pz)_2(CO)]\cdot 0.5pz$[d]	CH_3CN	585 (5100)	392 (7900)	253 (9 600)
$[Ru_3(O)(CH_3CO_2)_6(mbpy^+)_2(CO)](PF_6)_2$ (**1a**)	CH_3CN	590 (7800)	454 (6600)	260 (49 000)
	water	592 (6600)	388 (5700)	257 (42 600)

[a] Transitions between molecular orbitals arising from dπ(Ru)−pπ(μ_3-O) interactions within the Ru_3(μ_3-O) core. [b] Charge-transfer transitions from dπ−pπ orbitals of the Ru_3(μ_3-O) core to π^* orbitals of terminal ligands A. [c] $\pi-\pi^*$ transitions in terminal ligands A. [d] Absorption spectral data for a CH_2Cl_2 solution of $[Ru_3(O)(CH_3CO_2)_6(py)_2(CO)]$ and $[Ru_3(O)(CH_3CO_2)_6(pz)_2(CO)]$ are reported in refs 4 and 21, respectively.

orbitals in the triruthenium core to π^* orbitals of mbpy$^+$ ligands and L (cluster-to-ligand CT transitions). This assignment is supported by its large sensitivity to the variation of L; the band shifts to the longer wavelengths with increasing basicity of the third ligand. By contrast, the band I is relatively insensitive to the nature of the third terminal ligand L. The most intense band centered at 255−260 nm (band III) is ascribed to $\pi-\pi^*$ transitions of mbpy$^+$ ligands.

The CO complex **1a** shows three distinctive absorption bands at 590 nm (ϵ = 7800 $M^{-1}\,cm^{-1}$), 454 nm (ϵ = 6600 $M^{-1}\,cm^{-1}$), and 260 nm (ϵ = 49 000 $M^{-1}\,cm^{-1}$) in CH_3CN. The spectral pattern observed for **1a** is similar to that found in other mono(carbonyl) triruthenium analogs, $[Ru_3(O)(CH_3CO_2)_6(py)_2(CO)]$ and $[Ru_3(O)(CH_3CO_2)_6(pz)_2(CO)]$ (Table 5). For the valence-trapped $Ru^{III}_2Ru^{II}$ carbonyl complex, the band assignment analogous to that made for the Ru^{III}_3 complexes may not be possible, because the above dπ−pπ molecular orbital scheme is not applicable to this valence-trapped complex. However, a dπ−pπ molecular orbital scheme formed from two dπ(Ru^{III}) orbitals and one pπ(μ_3-O) orbital with less contribution from the "Ru^{II}−CO" moiety would be applicable for carbonyl complexes. Here we make band assignments for **1a** as follows: band I (λ_{max} = 590 nm) to intracluster (Ru_3O) transitions, band II (λ_{max} = 454 nm) to cluster(Ru_3O)-to-ligand-(mbpy$^+$) CT transitions, and band III (λ_{max} = 260 nm) to $\pi-\pi^*$(mbpy$^+$) transitions. These assignments are supported by the following considerations. First, the band II moves significantly upon substitution of non-carbonyl ligand (py, pz, and mbpy$^+$), while the other two transitions (bands I and III) are far less sensitive (Table 5). Second, band II in **1a** shifts remarkably upon changing the solvent from CH_3CN to water. This band (λ_{max} = 454 nm in CH_3CN) shifts to the shorter wavelength region in water (λ_{max} = 388 nm), while the other two transitions remain almost unchanged. A similar shift was also previously reported for the charge-transfer band for tris-(mbpy$^+$) triruthenium complex $[Ru^{III}_3(O)(CH_3CO_2)_6(mbpy^+)_3]^{4+}$ although the extent of shift was less (in CH_3CN, λ_{max} = 700 nm (ϵ = 8300 $M^{-1}\,cm^{-1}$), 395 nm (ϵ = 12 900 $M^{-1}\,cm^{-1}$),

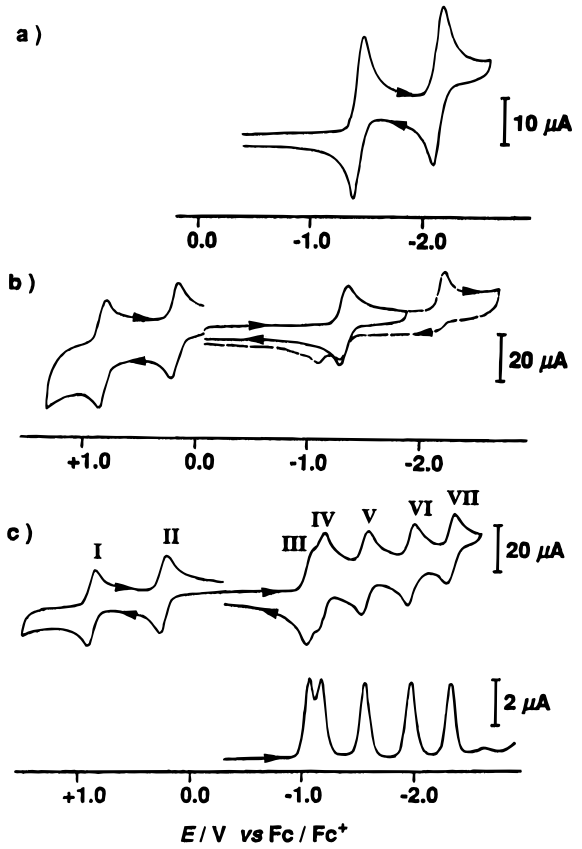

Figure 2. Cyclic voltammograms of (a) $[mbpy^+]PF_6$, (b) $[Ru_3(O)(CH_3CO_2)_6(py)_2(CO)]$, and (c) cyclic (upper) and differential-pulse voltammograms (lower) of $[Ru_3(O)(CH_3CO_2)_6(mbpy^+)_2(CO)](PF_6)_2$ (**1a**) in a 0.1 M $[(n\text{-}C_4H_9)_4N]PF_6-CH_3CN$ solution. Scan rate = 100 mV s^{-1} for CV and 20 mV s^{-1} for DPV.

and 255 nm (ϵ = 63 900 M^{-1} cm^{-1}); in water: λ_{max} = 700 nm (ϵ = 8300 M^{-1} cm^{-1}), 380 nm (sh, ϵ = 11 400 M^{-1} cm^{-1}), 330 nm (sh, ϵ = 14 700 M^{-1} cm^{-1}), and 252 nm (ϵ = 61 000 M^{-1} cm^{-1})).[27]

It should be noted that the spectral pattern of **1a** is appreciably different from those of electronically delocalized $Ru^{III}_2Ru^{II}$ complexes (an Ru oxidation number, +2.67) such as $[Ru^{III}_2Ru^{II}(O)(CH_3CO_2)_6(mbpy^+)_3](PF_6)_3$ (λ_{max} = 950, 570, 350 sh, and 260 nm in CH_3CN),[27] suggesting that the Ru_3 core of the CO analogs is in the valence-trapped state.

Also pointed out is a red-shift of the charge-transfer transitions (band II) for the $mbpy^+$ complexes $[Ru_3(O)(CH_3CO_2)_6(mbpy^+)_2(CO)](PF_6)_2$ (454 nm) and $[Ru_3(O)(CH_3CO_2)_6(mbpy^+)_2(pz)](PF_6)_3$ (380 nm) as compared to that of the corresponding transitions found in the pyridine analogs $[Ru_3(O)(CH_3CO_2)_6(py)_2(CO)]$ (333 nm) and $[Ru_3(O)(CH_3CO_2)_6(py)_2(pz)]PF_6$ (243 nm in CH_2Cl_2).[4] This is related to a lower π^* energy level of $mbpy^+$ over py.

5. Electrochemistry. Electrochemical properties of the mixed-terminal ligand triruthenium complexes were investigated by CV and DPV in a 0.1 M $[(n\text{-}C_4H_9)_4N]PF_6-CH_3CN$ solution.

a. Triruthenium Complexes with CO. A cyclic voltammogram and a differential-pulse voltammogram for $[Ru_3(O)(CH_3CO_2)_6(mbpy^+)_2(CO)](PF_6)_2$ (**1a**) are shown in Figure 2, part c. For comparison, cyclic voltammograms of the free ligand, $[mbpy^+]PF_6$, and $[Ru_3(O)(CH_3CO_2)_6(py)_2(CO)]$[37] under the same conditions are also displayed in Figure 2, parts a and b, respectively. Table 6 summarizes electrochemical data on the two complexes.

As seen in Figure 2, part a, the ligand $[mbpy^+]PF_6$ shows two reversible one-electron waves at $E_{1/2}$ = −1.33 and −2.02 V in a 0.1 M $[(n\text{-}C_4H_9)_4N]PF_6-CH_3CN$ solution. These processes are assignable to $mbpy^+/mbpy^\bullet$ and $mbpy^\bullet/mbpy^-$, respectively. The py complex $[Ru_3(O)(CH_3CO_2)_6(py)_2(CO)]$ shows three reversible waves in the range +2.0 to −1.8 V (as shown by a solid line in Figure 2, part b), which are due to consecutive one-electron redox on the $Ru_3(\mu_3\text{-}O)$ core: $Ru^{III}Ru^{IV}Ru^{III}(CO)/Ru^{III}_3$ ($E_{1/2}$ = +0.82 V), $Ru^{III}_3/Ru^{III}_2Ru^{II}(CO)$ ($E_{1/2}$ = +0.19 V), and $Ru^{III}_2Ru^{II}(CO)/Ru^{II}Ru^{III}Ru^{II}(CO)$ ($E_{1/2}$ = −1.33 V). When the scan range is extended toward the more negative region, one irreversible wave, $Ru^{II}Ru^{III}Ru^{II}(CO)/Ru^{II}_3$, is obtained at E_{pc} = −2.19 V, accompanied by an appearance of a new peak at E_{pa} = ca. −1.1 V in a back scan (a broken line in Figure 2, part b).

As shown in Figure 2, part c, the $mbpy^+$ complex **1a** exhibits a total of seven reversible waves, labeled I−VII. Each wave is a one-electron process as determined on the basis of the identical current intensity to the one-electron ferrocene/ferrocenium couple with the same concentration. On the basis of the comparison with redox potentials of the py complex (Figure 2, part b), it is evident that two waves in the positive region are due to consecutive redox on the Ru_3 core; process I ($E_{1/2}$ = +0.90 V) is to $Ru^{III}Ru^{IV}Ru^{III}(CO)/Ru^{III}_3$ and process II ($E_{1/2}$ = +0.26 V) is to $Ru^{III}_3/Ru^{III}_2Ru^{II}(CO)$. Both processes are electrochemically reversible at scan rates of $5 < \upsilon < 1000$ mV s^{-1}.

For the five waves in the negative region (III−VII), unambiguous assignments based on a comparison of the redox potentials of **1a** to reference compounds seemed to be difficult, since Ru_3 core-based redox potentials of CO complexes in the negative region are significantly influenced by the nature of terminal ligands.[39] To confirm the nature of these processes, spectroelectrochemical measurements were carried out by using an optically transparent thin-layer electrode (OTTLE) cell. Absorption spectra at applied potentials of the py complex $[Ru_3(O)(CH_3CO_2)_6(py)_2(CO)]$ and the $mbpy^+$ complex **1a** are shown in Figure 3, parts a and b, respectively. The numerical data are summarized in Table S-5 (supporting information). Controlled-potential absorption spectroscopic data have been described for some triruthenium complexes,[7,8,23,27] while those for CO complexes $[Ru_3(O)(CH_3CO_2)_6(L)_2(CO)]^{n-}$ have not been reported so far.

For $[Ru_3(O)(CH_3CO_2)_6(py)_2(CO)]$, two absorption bands ($\lambda_{max}$ = 580 and 330 nm) are observed at −0.6 V, a solid line in Figure 3, part a. This spectral pattern is consistent with that obtained for the isolated $Ru^{III}_2Ru^{II}$ complex. When the potential is applied at −1.7 V, where the one-electron reduced complex $[Ru^{II}Ru^{III}Ru^{II}(O)(CH_3CO_2)_6(py)_2(CO)]^-$ is generated (Figure 2, part b), a broad absorption band at λ_{max} = 1160 nm (ϵ = 4400 M^{-1} cm^{-1}) appears together with an absoption at 465 nm (ϵ = 9300 M^{-1} cm^{-1}) (Figure 3, part a, a broken line). The appearance of a near-infrared absorption is therefore a good indication of generation of the $Ru^{II}Ru^{III}Ru^{II}(CO)$ complex in solution. For **1a**, an absorption spectrum at −0.6 V consists of three bands at λ_{max} = 589 (ϵ = 7800 M^{-1} cm^{-1}), λ_{max} = 457 nm (ϵ = 6600 M^{-1} cm^{-1}), and λ_{max} = 257 nm (ϵ = 47 500 M^{-1} cm^{-1}), a solid line in Figure 3, part b. When the potential is set at −1.1 and −1.2 V (a midpoint potential of processes III and IV and processes IV and V in DPV, respectively, see Figure 2, part c), only a gradual decrease of intensity of the

(37) Redox potential data of this complex under the different conditions have been reported in refs 4 and 38.

(38) Ye, S.; Akutagawa, H.; Uosaki, K.; Sasaki, Y. *Inorg. Chem.* **1995**, *34*, 4527−4528.

(39) Hashimoto, M.; Hishikawa, M. Abe, M.; Sasaki, Y.; Ito, T. Unpublished results.

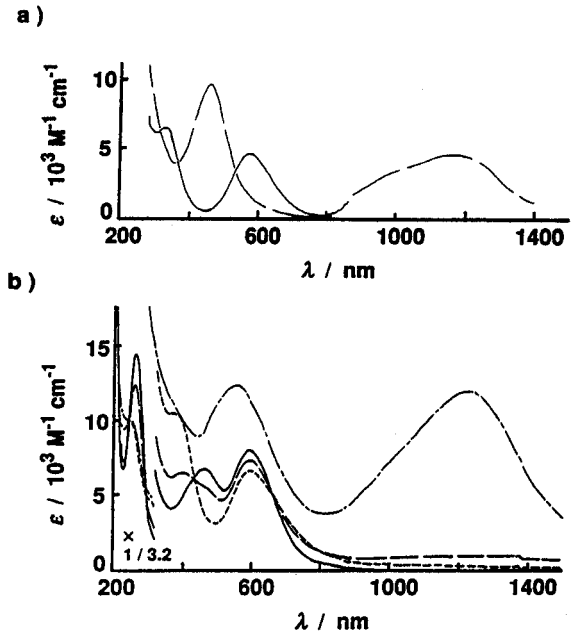

Figure 3. Controlled-potential absorption spectra of (a) $[Ru_3(O)(CH_3CO_2)_6(py)_2(CO)]$ and (b) $[Ru_3(O)(CH_3CO_2)_6(mbpy^+)_2(CO)](PF_6)_2$ (**1a**) in a 0.1 M $[(n\text{-}C_4H_9)_4N]PF_6-CH_3CN$ solution: (a) solid line, −0.6 V; dashed line, −1.7 V; (b) solid line, −0.6 V; dotted line, −1.1 V; dashed line, −1.2 V; dashed-dotted line, −1.6 V *vs* Fc/Fc^+.

Table 6. Electrochemical Data of $[Ru_3(O)(CH_3CO_2)_6(mbpy^+)_2(CO)](PF_6)_2$ (**1a**) and $[Ru_3(O)(CH_3CO_2)_6(py)_2(CO)]$ in 0.1 M $[(n\text{-}C_4H_9)_4N]PF_6-CH_3CN$[a]

		$E_{1/2}$,[b] V *vs* Fc/Fc^+ (ΔE_p[c]), *ne*[d]	
redox wave	assignment	$(mbpy^+)_2(CO)$, **1a**	$(py)_2(CO)$
I	$Ru^{III}Ru^{IV}Ru^{III}(CO)/Ru^{III}_3$	+0.90 (60), 1e	+0.82 (60), 1e
II	$Ru^{III}_3/Ru^{III}_2Ru^{II}(CO)$	+0.26 (60), 1e	+0.19 (60), 1e
III	$(mbpy^+)_2/(mbpy^+)(mbpy^\bullet)$	−1.07,[e] 1e	
IV	$(mbpy^+)(mbpy^\bullet)/(mbpy^\bullet)_2$	−1.17,[e] 1e	
V	$Ru^{III}_2Ru^{II}(CO)/Ru^{III}Ru^{II}Ru^{II}(CO)$	−1.56 (50), 1e	−1.33 (50), 1e
VI	$(mbpy^\bullet)_2/(mbpy^\bullet)(mbpy^-)$	−1.97 (50), 1e	
VII	$(mbpy^\bullet)(mbpy^-)/(mbpy^-)_2$	−2.32 (60), 1e	
VIII	$Ru^{III}Ru^{II}Ru^{II}(CO)/Ru^{II}_3$	−2.99,[f] 1e	−2.19,[f] 1e

[a] Data from cyclic voltammograms obtained at +22 ± 1 °C at a scan rate of 100 mV s^{-1} by using a glassy carbon working electrode, a platinum coil counter electrode, and an Ag/Ag^+ ($[AgClO_4]$ = 0.01 M in CH_3CN) reference electrode. [Complex] = 1 mM. All potentials are reported *vs* Fc/Fc^+ couple. [b] $E_{1/2} = (E_{pa} + E_{pc})/2$, where E_{pa} and E_{pc} are anodic and cathodic peak potentials, respectively. [c] $\Delta E_p = E_{pa} - E_{pc}$. [d] *ne* = no. of electrons exchanged. [e] Peak potential in DPV. [f] E_{pc} value for irreversible process.

589 nm-band and a blue-shift of the 457-nm band are observed. These suggest that the two one-electron processes III and IV are concerned with redox on $mbpy^+$ ligands alone and not on the $Ru_3(\mu_3\text{-}O)$ core. As has been reported, one-electron reduction of $mbpy^+$ gives rise to two absorption bands at λ_{max} = 369 and 535 nm under the same conditions.[27] If the potential is applied at −1.6 V (between processes V and VI), a drastic increase of an absorption with λ_{max} = 1213 nm (ϵ = 11 700 M^{-1} cm^{-1}) is then observed. The appearance of the strong near-infrared band indicates one-electron reduction of the $Ru^{III}_2Ru^{II}(CO)$ core occurs in process V. Further information on processes VI and VII, as well as on an irreversible process VIII (E_p = −2.99 V; not shown in Figure 2, part c, see Table 6), was not obtained because of the instability of such highly reduced complexes. However, the most plausible assignments are the consecutive two one-electron reductions of $mbpy^\bullet$ ligands occurring at VI and VII and the one-electron reduction of the $Ru^{II}Ru^{III}Ru^{II}(CO)$ core at VIII. These assignments are based on the the higher reversibility of the ligand-based process and irreversible nature of the $Ru^{II}Ru^{III}Ru^{II}(CO)/Ru^{II}_3$ process as found in $[Ru_3(O)(CH_3CO_2)_6(py)_2(CO)]$ (Figure 2, part a). The significantly negative shift of the latter core-based process in **1a** relative to that in the py analog (800 mV) is primarily due to the highly negative charge for this process in complex **1a** (−3/−4).

Redox processes of the CO complex can be summarized as shown in Scheme 1. Here, the last Ru in the formula in the mixed-valent complexes represents the Ru that is coordinated by CO.

Scheme 1

$$[Ru^{III}Ru^{IV}Ru^{III}(O)(CH_3CO_2)_6(mbpy^+)_2(CO)]^{4+}$$

$$+1e^- \downarrow\uparrow -1e^- \quad \text{(I)}$$

$$[Ru^{III}_3(O)(CH_3CO_2)_6(mbpy^+)_2(CO)]^{3+}$$

$$+1e^- \downarrow\uparrow -1e^- \quad \text{(II)}$$

$$[Ru^{III}_2Ru^{II}(O)(CH_3CO_2)_6(mbpy^+)_2(CO)]^{2+}$$

$$+1e^- \downarrow\uparrow -1e^- \quad \text{(III)}$$

$$[Ru^{III}_2Ru^{II}(O)(CH_3CO_2)_6(mbpy^\bullet)(mbpy^+)(CO)]^{+}$$

$$+1e^- \downarrow\uparrow -1e^- \quad \text{(IV)}$$

$$[Ru^{III}_2Ru^{II}(O)(CH_3CO_2)_6(mbpy^\bullet)_2(CO)]$$

$$+1e^- \downarrow\uparrow -1e^- \quad \text{(V)}$$

$$[Ru^{II}Ru^{III}Ru^{II}(O)(CH_3CO_2)_6(mbpy^\bullet)_2(CO)]^{-}$$

$$+1e^- \downarrow\uparrow -1e^- \quad \text{(VI)}$$

$$[Ru^{II}Ru^{III}Ru^{II}(O)(CH_3CO_2)_6(mbpy^-)(mbpy^\bullet)(CO)]^{2-}$$

$$+1e^- \downarrow\uparrow -1e^- \quad \text{(VII)}$$

$$[Ru^{II}Ru^{III}Ru^{II}(O)(CH_3CO_2)_6(mbpy^-)_2(CO)]^{3-}$$

$$+1e^- \downarrow \quad \text{(VIII)}$$

$$[Ru^{II}_3(O)(CH_3CO_2)_6(mbpy^-)_2(CO)]^{4-}$$

Two-step one-electron ligand redox processes in **1a** (III and IV for $mbpy^+/mbpy^\bullet$ and VI and VII for $mbpy^\bullet/mbpy^-$) reflect the existence of terminal ligand−ligand interactions as discussed below.

b. Triruthenium Complexes with L (L = H_2O, pz, py, Him, and dmap). Redox potentials for five mixed-ligand triruthenium(III) complexes differ significantly from those for the carbonyl complex **1a** but resemble those for the previously described tris$(mbpy^+)$triruthenium(III) complex $[Ru_3(O)(CH_3CO_2)_6(mbpy^+)_3]^{4+}$.[27] Figure 4 shows the cyclic voltammogram and differential-pulse voltammogram of $[Ru_3(O)(CH_3CO_2)_6(mbpy^+)_2(pz)](PF_6)_3$ (**3a**) as a typical example. Redox potential data as well as their assignments on **2a**−**6b** are tabulated in Table 7.

Table 7. Electrochemical Data for the Triruthenium Complexes $[Ru_3(O)(CH_3CO_2)_6(mbpy^+)_2(L)]^{3+}$ (L = H_2O, pz, py, Him, and dmap) in 0.1 M $[(n\text{-}C_4H_9)_4N]PF_6-CH_3CN$[a]

		$E_{1/2}$[b], V *vs* Fc/Fc^+ (ΔE_p[c]), *ne*[d]				
redox wave	assignment	H_2O (**2a**)	pz (**3a**)	py (**4b**)	Him (**5a**)	dmap (**6b**)
I	$Ru^{IV}_2Ru^{III}/Ru^{IV}Ru^{III}_2$	+1.72,[e] 1e	+1.65 (100),[f] 1e	+1.65,[e] 1e	+1.57,[e] 1e	+1.55,[e] 1e
II	$Ru^{IV}Ru^{III}_2/Ru^{III}_3$	+0.69 (60), 1e	+0.67 (60), 1e	+0.63 (60), 1e	+0.58 (60), 1e	+0.56 (40), 1e
III	$Ru^{III}_3/Ru^{III}_2Ru^{II}$	−0.32 (50), 1e	−0.33 (50), 1e	−0.38 (50), 1e	−0.43 (40), 1e	−0.44 (50), 1e
IV	$(mbpy^+)_2/(mbpy^\bullet)_2$	−1.27 (80), 2e	−1.26 (80), 2e	−1.28 (80), 2e	−1.31 (90), 2e	−1.31 (100), 2e
V	$Ru^{III}_2Ru^{II}/Ru^{III}Ru^{II}_2$	−1.68 (60), 1e	−1.64 (50), 1e	−1.72 (40), 1e	−1.78 (60), 1e	−1.78 (60), 1e
VI	$(mbpy^\bullet)_2/(mbpy^\bullet)(mbpy^-)$	−2.01 (50), 1e	−2.00 (50), 1e	−1.99 (40), 1e	−2.02 (20),[f] 1e	−2.02 (50), 1e
VII	$(mbpy^\bullet)(mbpy^-)/(mbpy^-)_2$	−2.47, 1e	−2.36 (50), 1e	−2.49, 1e	−2.42 (60)[g]	−2.56 (60), 1e
VIII	$Ru^{III}Ru^{II}_2/Ru^{II}_3$		−2.80, 1e[e]	−2.78, 1e[e]	−2.70,[h] 1e	−2.97,[e] 1e

[a] Data from cyclic voltammograms obtained at +22 ± 1 °C at a scan rate of 100 mV s^{-1} by using a glassy carbon working electrode, a platinum coil counter electrode, and an Ag/Ag^+ ($[AgClO_4]$ = 0.01 M in CH_3CN) reference electrode. [Complex] = 1 mM. All potentials are reported *vs* Fc/Fc^+ couple. [b] $E_{1/2} = (E_{pa} + E_{pc})/2$, where E_{pa} and E_{pc} are anodic and cathodic peak potentials, respectively. [c] $\Delta E_p = E_{pa} - E_{pc}$. [d] *ne* = no. of electrons exchanged. [e] E_{pc} value for irreversible process. [f] Quasireversible process. [g] Current intensity of the process is smaller as compared to that of the other one-electron processes. [h] Peak potential in DPV.

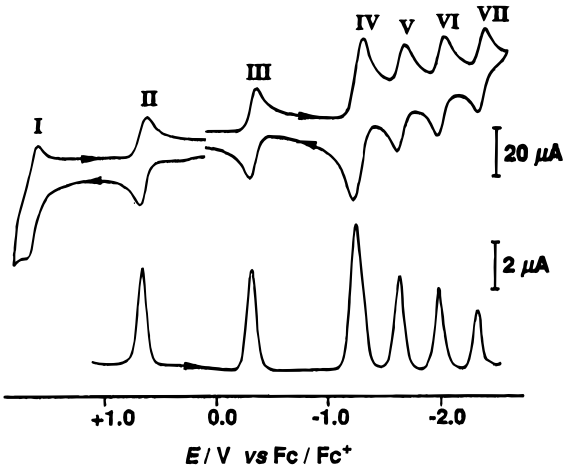

Figure 4. Cyclic (upper) and differential-pulse voltammograms (lower) of $[Ru_3(O)(CH_3CO_2)_6(mbpy^+)_2(pz)](PF_6)_3$ (**3a**) in a 0.1 M $[(n\text{-}C_4H_9)_4N]PF_6-CH_3CN$ solution. Scan rate = 100 mV s^{-1} for CV and 20 mV s^{-1} for DPV.

The pz complex **3a** exhibits seven redox waves including one quasi-reversible wave (process I) and six reversible waves (processes II−VII) in the range +2.0 to −2.6 V *vs* Fc/Fc^+. Comparison of the $E_{1/2}$ values with those for the tris($mbpy^+$) complex allows us to assign processes I, II, III, and V to a successive redox of the $Ru_3(\mu_3\text{-}O)$ core. Process IV, which, on the basis of the current intensity, involves two electrons, is due to reduction of two terminal ligands, $mbpy^+/mbpy^\bullet$. The last two processes VI and VII are best ascribed to the ligand-based processes $mbpy^\bullet/mbpy^-$. An irreversible wave found in the most negative potential (process VIII in Table 7) is due to the reduction of the trinuclear core $Ru^{II}_2Ru^{III}/Ru^{II}_2$, which would involve a loss of the central oxide ion as claimed for other triruthenium complexes.[2,7]

For complexes **2a** (L = H_2O), **4b** (py), and **6b** (dmap), seven reversible waves involving eight electrons are also observed. Complex **5a** (L = Him) also shows seven waves, but their reversibility is lowered. As can be seen in Table 7, Ru_3 core-based redox couples shift negatively upon changing L into a more electron-donating ligand, while the ligand-based couple shifts to a lesser extent. This indicates that $d\pi-p\pi$ molecular orbital levels in the trimetal core are more sensitive to the nature of L than to the π^* levels of $mbpy^+$.

Redox processes of mixed-ligand triruthenium(III) complexes (**2a**, **3a**, **4b**, **5a**, and **6b**) can be thus summarized as shown in Scheme 2.

Scheme 2

$$[Ru^{III}Ru^{IV}_2(O)(CH_3CO_2)_6(mbpy^+)_2(L)]^{5+}$$

$$+1e^- \downarrow\uparrow -1e^- \qquad \text{(I)}$$

$$[Ru^{III}_2Ru^{IV}(O)(CH_3CO_2)_6(mbpy^+)_2(L)]^{4+}$$

$$+1e^- \downarrow\uparrow -1e^- \qquad \text{(II)}$$

$$[Ru^{III}_3(O)(CH_3CO_2)_6(mbpy^+)_2(L)]^{3+}$$

$$+1e^- \downarrow\uparrow -1e^- \qquad \text{(III)}$$

$$[Ru^{II}Ru^{III}_2(O)(CH_3CO_2)_6(mbpy^+)_2(L)]^{2+}$$

$$+(1e^-+1e^-) \downarrow\uparrow -(1e^-+1e^-) \qquad \text{(IV)}$$

$$[Ru^{II}Ru^{III}_2(O)(CH_3CO_2)_6(mbpy^\bullet)_2(L)]$$

$$+1e^- \downarrow\uparrow -1e^- \qquad \text{(V)}$$

$$[Ru^{II}_2Ru^{III}(O)(CH_3CO_2)_6(mbpy^\bullet)_2(L)]^-$$

$$+1e^- \downarrow\uparrow -1e^- \qquad \text{(VI)}$$

$$[Ru^{II}_2Ru^{III}(O)(CH_3CO_2)_6(mbpy^-)(mbpy^\bullet)(L)]^{2-}$$

$$+1e^- \downarrow\uparrow -1e^- \qquad \text{(VII)}$$

$$[Ru^{II}_2Ru^{III}(O)(CH_3CO_2)_6(mbpy^-)_2(L)]^{3-}$$

$$+1e^- \downarrow \qquad \text{(VIII)}$$

$$[Ru^{II}_3(CH_3CO_2)_6(mbpy^-)_2(L)]^{2-} + O^{2-}$$

In contrast to the splitting behavior of the $mbpy^+/mbpy^\bullet$ process for the CO complex **1a** in the cyclic voltammogram, the corresponding processes for **2a**−**6b** are observed as a single wave, indicating much smaller interactions between ligands. However, a subtle difference in redox behavior of this process among **2a**−**6b** can be observed in the differential-pulse voltammograms as shown in Figure 5. While the ligand-based process for the pz (**3a**) and py (**4b**) complexes as well as that for the aqua complex (**2a**) is still detected as an unresolved wave,

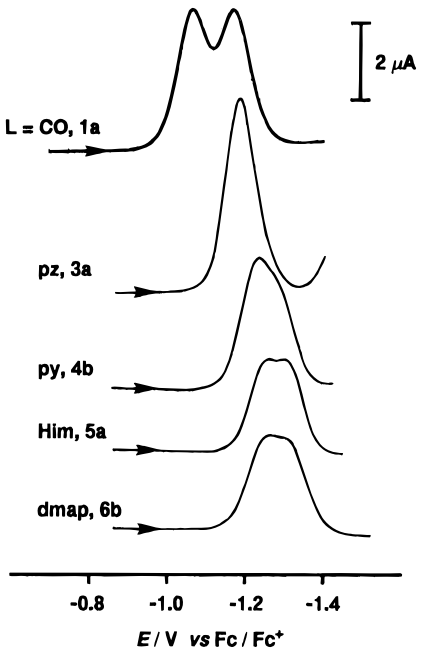

Figure 5. Differential-pulse voltammograms for the $mbpy^+/mbpy^•$ process of the mixed-ligand Ru_3 complexes $[Ru_3(O)(CH_3CO_2)_6(mbpy^+)_2(CO)]^{2+}$ and $[Ru_3(O)(CH_3CO_2)_6(mbpy^+)_2(L)]^{3+}$ (L = pz, py, Him, and dmap) in a 0.1 M $[(n\text{-}C_4H_9)_4N]PF_6-CH_3CN$ solution. Scan rate = 20 mV s^{-1}.

two resolved waves (ΔE_p = ca. 40 mV) are observed for the Him (**5a**) and dmap (**6b**) complexes. Among the series, the carbonyl complex exhibits the largest peak split (ΔE_p = ca. 100 mV). From these voltammograms, the difference in $E_{1/2}$ values between two closely spaced ligand−redox waves ($\Delta E_{1/2}$) is estimated.[40] $\Delta E_{1/2}$ values thus obtained are 28 mV (K_{com} = 3.0) for **2a**, 37 mV (K_{com} = 4.2) for **3a**, 68 mV (K_{com} = 14.1) for **4b**, 73 mV (K_{com} = 17.1) for **5a**, 80 mV (K_{com} = 22.5) for **6b**, and 100 mV (K_{com} = 95.0) for **1a**. The values show a tendency that the splitting of ligand-based waves increases as the more basic ligand becomes coordinated at the third terminal position. The split for the aqua and pz complexes is comparable to that estimated for the statistical potential difference in noninteracting redox-active centers ($\Delta E_{1/2}$ = 36 mV),[41] while the splits for the py, Him, dmap, and CO complexes definitely exceed the value and show the occurrence of electronic interactions between terminal ligands.[42]

Discussion

1. Electronic Structure of Ru_3 Complexes. It has been pointed out that mono(carbonyl)triruthenium $Ru^{II}Ru^{III}_2$ complexes exhibit considerably different spectroscopic and redox properties from other members of the triruthenium $Ru^{II}Ru^{III}_2$ complexes.[4,11,38] On the basis of the present X-ray analysis on **1b**·2DMF, the elecronic structure of the CO complexes is best described as being in the valence-trapped $Ru^{III}_2Ru^{II}(CO)$ oxidation state, in which the divalent state is localized on the Ru site bonded with CO. This is interpreted as a consequence of a strong back-donating property of the CO ligand. From the spectroscopic similarities among **1b** and other CO derivatives, the mono(carbonyl)triruthenium core is considered to have the same localized-elecronic state irrespective of the kind of the remaining two terminal ligands. The valence-trapped nature was also suggested by a recent infrared spectroelectrochemical study on $[Ru_3(O)(CH_3CO_2)_6(py)_2(CO)]$[38] and terminal ligand-substitution kinetics for $[Ru_3(O)(CH_3CO_2)_6(py)_2(CO)]$ and $[Ru_3(O)(CH_3CO_2)_6(py)_3]^{0/+}$.[11] The analogous valence-trapped character for the oxo-centered trinuclear complex has been shown for $[Mn^{III}_2Mn^{II}(O)(C_6H_5CO_2)_6(py)_2(H_2O)]\cdot 0.5CH_3CN$,[43] as well as for several trimanganese and triiron complexes at lower temperatures.[44]

By contrast, in the mixed-ligand complxes **2a**−**6b**, one unpaired electron in the Ru^{III}_3 core is considered to be essentially delocalized over three Ru ions. This is supported by close similarities of their absorption spectral patterns, ^1H NMR chemical shifts, and redox potentials to those found in delocalized triruthenium complexes such as $[Ru^{III}_3(O)(CH_3CO_2)_6(mbpy^+)_3]^{4+}$ [27] and $[Ru^{III}_3(O)(CH_3CO_2)_6(py)_3]^+$.[4]

2. Multistep Redox Properties. In this study, redox behavior of mixed-ligand Ru_3 complexes has been investigated in detail by means of cyclic and differential-pulse voltammetry together with controlled-potential absorption spectral measurements. The present complexes are found to show tunable multistep redox properties. The CO complex **1a** exhibits eight one-electron steps involving seven reversible waves, while Ru^{III}_3 complexes with aqua (**2a**) and *N*-heterocyclic terminal ligand (**3a**−**6b**) display seven−eight reversible waves in CH_3CN. Among these series, spectroscopic and redox properties of the CO complex differ significantly from those found in the other complexes with L. Introduction of a terminal CO ligand causes the triruthenium core to be more difficult to oxidize and easier to reduce. This trend is consistent with previous observations for other triruthenium complexes.

3. Ligand−Ligand Interactions. One of the most interesting characteristics of the present $mbpy^+$-coordinated triruthenium complexes would be the occurrence of the ligand−ligand interactions between two $mbpy^+$ ligands, as manifested by the splitting of ligand-based redox waves on voltammograms. This interaction is due to electronic $\pi-\pi$ coupling of ligands through the Ru(dπ)−(μ_3-O)(pπ)−Ru(dπ) pathway to which $mbpy^+$ ligands are coordinated. Recent magnetic study on oxo-centered acetate-bridged trimetal complexes has indicated that $Ru^{III}\cdots Ru^{III}$ interactions via the central μ_3-oxide bridge is dominant over interactions involving μ-acetate bridges in $[Ru^{III}_2Rh^{III}(O)(CH_3CO_2)_6(py)_3]^+$ and $[Ru^{III}_2Ru^{II}(O)(CH_3CO_2)(py)_3]$, both of which are isoelecronic to the present CO complex ($d^5d^5d^6$).[16b] We previously showed electronic interactions among three $mbpy^+$ ligands in tris($mbpy^+$) analogs, $[M_3(O)(CH_3CO_2)_6(mbpy^+)_3]^{4+}$ (M_3 = Ru_3, Rh_3, and Ru_2Rh).[27] In particular, the mixed Ru_2Rh complex showed the largest interactions with three split ligand-reduction waves at $E_{1/2}$ = −1.14, −1.26, and −1.45 V *vs* Fc/Fc^+ in CH_3CN. This strong interaction was explained by considering not only different metal sites (Ru and

(40) Richardson, D. E.; Taube, H. *Inorg. Chem.* **1981**, *20*, 1278−1285.
(41) Flanagan, J. B.; Margel, S.; Bard, A. J.; Anson, F. C. *J. Am. Chem. Soc.* **1978**, *100*, 4248−4253.
(42) Vleček, A. A. *Coord. Chem. Rev.* **1982**, *42*, 39−62.
(43) Vincent, J. B.; Chang, H.-R.; Folting, K.; Huffman, J. C.; Christou, G.; Hendrickson, D. N. *J. Am. Chem. Soc.* **1987**, *109*, 5703−5711.
(44) Hendrickson and co-workers have reported interconversion between valence-trapped and -detrapped electronic states in the trinuclear mixed-valent complexes $[M_3(O)(CH_3CO_2)_6L_3]\cdot S$ (M_3 = $Mn^{II}Mn^{III}_2$, $Fe^{II}Fe^{III}_2$; L = neutral ligand such as py, S = solvent molecule): (a) Jang, H. G.; Geib, S. J.; Kaneko, Y.; Nakano, M.; Sorai, M.; Rheingold, A. L.; Montez, B.; Hendrickson, D. N. *J. Am. Chem. Soc.* **1989**, *111*, 173−186. (b) Kaneko, Y.; Nakano, M.; Sorai, M.; Jang, H. G.; Hendrickson, D. N. *Inorg. Chem.* **1989**, *28*, 1067−1073. (c) McCusker, J. K.; Jang, H. G.; Zvagulis, M.; Ley, W.; Hendrickson, D. N. *Inorg. Chem.* **1991**, *30*, 1985−1990. (d) Nakano, M; Sorai, M.; Vincent, J. B.; Christou, G.; Jang, H. G.; Hendrickson, D. N. *Inorg. Chem.* **1989**, *28*, 4608−4614. (e) Jang, H. G.; Vincent, J. B.; Nakano, M.; Huffman, J. C.; Christou, G.; Sorai, M.; Wittebort, R. J.; Hendrickson, D. N. *J. Am. Chem. Soc.* **1989**, *111*, 7778−7784. (f) McCusker, J. K.; Jang, H. G.; Wang, S.; Christou, G.; Hendrickson, D. N. *Inorg. Chem.* **1992**, *31*, 1874−1880.

Rh) but also interactions between two $mbpy^+$ ligands through vacant $d\pi-p\pi$ orbitals.[27] The analogous interactions may be possible for the present mixed-ligand Ru_3 complexes.

The largest interactions observed for the CO complex can be interpreted in terms of both structural and electronic factors as follows. First, the extremely short $(mbpy^+)Ru-(\mu_3\text{-}O)$ distance (1.894(6) Å) causes stronger interactions between two Ru sites through the central oxide bridge. It is highly likely that larger $Ru-(\mu_3\text{-}O)$ interactions induce larger interactions between two $mbpy^+$ ligands, since the $\pi^*(mbpy^+)$ orbitals can appropriately match d_{yz} (Ru) orbitals in symmetry.[45] Second, the electronically localized $Ru^{III}-O-Ru^{III}$ moiety also seems to play an important role. Strong electronic and magnetic interactions between two Ru^{III} sites through the central oxide have been previously shown in the mixed-metal trinuclear complexes $[Ru_2Cr(O)(CH_3CO_2)_6(py)_3]^+$ [17] and $[Ru_2M(O)(CH_3CO_2)_6(L)_3]$ (M = Mg, Mn, Co, Ni, Zn; L = H_2O, py).[16a] As stated above, the present CO complex may be also considered to involve an electronically localized $Ru^{III}-O-Ru^{III}$ moiety rather than a delocalized $Ru^{+2.67}{}_3(\mu_3\text{-}O)$ one. This would contribute to the larger interactions between two Ru sites and hence between two $mbpy^+$ ligands in the CO complex. In addition, for the mixed-ligand triruthenium(III) complexes (**3a**−**6b**), a negative shift of $E_{1/2}$ values of $Ru_3(\mu_3\text{-}O)$ core-based processes is evident upon substituting L with more basic ligands L (Table 7). This suggests that the HOMO level of the trinuclear cluster core approaches to the π^* level of $mbpy^+$ on going from L = pz to dmap, which would also provide increasing extent of interactions between metal and ligand redox sites.

Conclusion

The present study has shown reversible multistep and multielectron redox behavior of cluster complexes comprised of oxo-centered acetate-bridged triruthenium unit and two redox-active terminal ligands *N*-methyl-bipyridinium ions ($mbpy^+$) $[Ru_3(O)(CH_3CO_2)_6(mbpy^+)_2(L)]^{2+/3+}$ (L = a monodentate neutral ligand). Introduction of the 2/1 mixed-terminal ligand composition enables us to construct unique triruthenium complexes bearing tunable spectroscopic and redox properties. These complexes show at least seven reversible waves in the cyclic voltammograms, involving eight−nine electrons which are $Ru_3(\mu_3\text{-}O)$ core-based and terminal ligand-based ($mbpy^+/mbpy^\bullet$, $mbpy^\bullet/mbpy^-$). Across the series, the CO complex is characterized as being in the valence-trapped $Ru^{III}{}_2Ru^{II}(CO)$ oxidation state on the basis of the significant differences between two types of Ru···Ru distances (Ru···Ru(CO) = 3.410(2) Å, Ru···Ru = 3.276(2) Å) together with notably different absorption spectral pattern from that observed for delocalized $Ru^{III}{}_2Ru^{II}$ analogs. Most interestingly, intramolecular electronic interactions between two $mbpy^+$ ligands exist in the present Ru_3 complexes; introduction of a CO ligand or basic *N*-heterocyclic ligands (imidazole and 4-(dimethylamino)pyridine) as the third terminal ligand causes more significant interactions. This interaction can be interpreted as occurring through the Ru−O−Ru $d\pi-p\pi$ pathway. Large interactions between ligands found for the CO complex are concluded to be primarily due to the more significant extent of $\pi^*(mbpy^+)-d\pi(Ru)-p\pi(\mu_3\text{-}O)$ overlap caused by the shorter $(mbpy^+)Ru^{III}-O$ distance (1.894(6) Å).

Acknowledgment. This work was supported by Grant-in-Aids for Scientific Research Grants 03231105 (Y.S.), 03241106 and 03555184 (S.Y.), and 02303006, 04453041, and 04241104 (T.I.) from the Ministry of Education, Science, and Culture, Japan. S.Y. acknowledges the Nihon-itagarasu Foundation and the Iwatani Naoji Foundation for financial support. The authors also acknowledge Professor Hiroaki Kido for valuable discussions.

Supporting Information Available: Tables of full crystallographic data, positional and equivalent isotropic displacement parameters for non-hydrogen and hydrogen atoms, anisotropic displacement parameters, ORTEP drawings for **1b**·2DMF, and controlled-potential absorption spectral data for $[Ru_3(O)(CH_3CO_2)_6(py)_2(CO)]$ and **1a** (7 pages). See any current masthead page for ordering information.

IC960430J

(45) We assume that the $mbpy^+$ ligand at the terminal position freely rotate along the Ru−N bond. The largest orbital overlap between d_{yz}(Ru) and $\pi^*(mbpy^+)$ is expected when the aromatic plane is parallel to the $Ru_3(\mu_3\text{-}O)$ plane.